

# Size-mediated cytotoxicity of nanocrystalline titanium dioxide, pure and zinc-doped hydroxyapatite nanoparticles in human hepatoma cells

G. Devanand Venkatasubbu · S. Ramasamy ·  
G. S. Avadhani · L. Palanikumar · J. Kumar

Received: 18 October 2011 / Accepted: 9 March 2012 / Published online: 30 March 2012  
© Springer Science+Business Media B.V. 2012

**Abstract** Nanoparticles are highly used in biological applications including nanomedicine. In this present study, the interaction of HepG2 hepatocellular carcinoma cells (HCC) with hydroxyapatite (HAp), zinc-doped hydroxyapatite, and titanium dioxide (TiO<sub>2</sub>) nanoparticles were investigated. Hydroxyapatite, zinc-doped hydroxyapatite and titanium dioxide nanoparticles were prepared by wet precipitation method. They were subjected to isochronal annealing at different temperatures. Particle morphology and size distribution were characterized by X-ray diffraction and transmission electron microscope. The nanoparticles were co-cultured with HepG2 cells. MTT assay was employed to evaluate the proliferation of tumor cells. The DNA damaging effect of HAp, Zn-doped HAp, and TiO<sub>2</sub> nanoparticles in human hepatoma cells (HepG2) were evaluated using DNA fragmentation studies. The results showed that in HepG2 cells, the anti-tumor activity strongly depend on the size of nanoparticles in HCC cells. Cell cycle arrest analysis for HAp, zinc-doped HAp, and TiO<sub>2</sub> nanoparticles revealed the influence of HAp, zinc-

doped HAp, and titanium dioxide nanoparticles on the apoptosis of HepG2 cells. The results imply that the novel nano nature effect plays an important role in the biomedical application of nanoparticles.

**Keywords** Hydroxyapatite · Zinc-doped hydroxyapatite · Titanium dioxide · Human Hepatoma cells · DNA fragmentation · Toxicity · Environmental and health effects

## Introduction

Nanomaterials are important materials due to their novel characteristics, unique physical and chemical properties. Some identified nanoparticles have anti-cancer activity. It is by the accumulation of the nanoparticles in the cell by enhanced permeability and retention effect (Sheng et al. 2005; Lee et al. 2010). Due to these changes the nanoparticles achieve new biological properties (Kasemets et al. 2009). Hepatocellular carcinoma (HCC), the most common primary malignant tumor of the liver, is a serious threat to human life. Progress in diagnosis and chemical and radiation therapies are poor. Tumor cells are capable of rapid proliferation, local invasion, and distance migration. It was almost impossible to excise malignant tumor completely. So we need to find out new materials for treatment. Nanoparticles and molecules are a potential alternative for treatment of disease

---

G. Devanand Venkatasubbu · S. Ramasamy (✉) ·  
L. Palanikumar · J. Kumar  
Crystal Growth Centre, Anna University,  
Chennai 600025, Tamil Nadu, India  
e-mail: sinna\_ramasamy@yahoo.com

G. S. Avadhani  
Department of Materials Engineering, Indian Institute  
of Science, Bangalore, India

because of their unique biological effect. Zinc oxide nanoparticles have anticancer activity against human myeloblastic leukemia cells (Premanathan et al. 2011). The anticancer activity of chitosan is well studied (Lifeng Qi et al. 2001). Nanocrystalline fullerenes have anticancer activity against human glioma cell line (Harhaji et al. 2007). Nickel oxide nanoparticles are found to have anticancer activity against human lung carcinoma cells (Horie et al. 2009). Genetic material is delivered into the cell by gene delivery to modify the cell (Hosseinkhani 2006). DNA nanoparticles were used for the delivery of genetic materials (Hosseinkhani et al. 2011). Due to the unique structural character and properties inorganic nanoparticles are used in medical field. The effect of morphology, size, and ions substitution of the inorganic nanoparticles on the cancer cells are very important. The cellular uptake of the nanoparticles and their anticancer activity depends upon the particle size. The anticancer activity of the nanoparticles varies with the size and surface area of the nanoparticles (Liu et al. 2003; Yin et al. 2006; Li et al. 2008).

Hydroxyapatite ( $\text{Ca}_{10}(\text{PO}_4)_6(\text{OH})_2$ , HAP), is of much interest since it is the structural template for the mineral material in human and animal bones. It is biocompatible, biodegradable and has close similarity with the inorganic component of vertebrate bone (Bohner, 2001; Ong et al. 2008). Hydroxyapatite nanoparticles are used as drug delivery system for various classes of drugs, proteins, and enzymes (Jntema et al. 1994; Reibeiro et al. 2004). Hydroxyapatite is usually doped with different trace elements to increase its biological activity. Zinc, an important trace element in all biological tissues, takes part in the activity of more than 300 types of enzymes (de Lima et al. 2006). Zinc-doped hydroxyapatite nanoparticles are biocompatible and have increased bioactivity. Titanium dioxide ( $\text{TiO}_2$ ) nanoparticles are used in medical applications due to their biocompatibility. In vivo toxicological analysis shows that titanium dioxide nanoparticles are non toxic (Wang et al. 2011). Titanium dioxide nanoparticles in bulk form are biologically inert. But when titanium dioxide is prepared below size less than 20 nm, it readily binds enediol bidentate ligands including dopamine, ascorbic acid, alizarin, and alizarin red S. The size, shape, and aggregation of titanium dioxide nanoparticles are

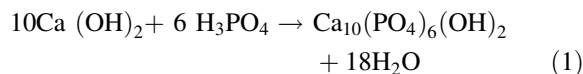
important factors in the anticancer activity of titanium dioxide nanoparticles.

In this study we have synthesized pure hydroxyapatite, zinc-doped hydroxyapatite, and titanium dioxide nanoparticles of various sizes. The phase composition, morphology, size, and incorporation of zinc into hydroxyapatite were studied using X-ray diffraction (XRD) and transmission electron microscopy (TEM). The structural and functional effect of the nanoparticles on hepatocellular carcinoma cells in vitro were investigated. This cell line was selected since hepatoma is one of the most common tumors found worldwide. Further in primary malignancy of the liver this cell line has been widely used as the human hepatoma model cell line in the development of new anti-tumor medicines. The long-term aim of the present study is to find an alternative cancer therapy with fewer side effects for healthy cells.

## Materials and methods

### Synthesis of hydroxyapatite and Zinc-doped hydroxyapatite nanoparticles

Hydroxyapatite nanoparticles were synthesized by wet chemical precipitation reaction:



Aqueous suspension of calcium hydroxide ( $\text{Ca}(\text{OH})_2$ ) and orthophosphoric acid ( $\text{H}_3\text{PO}_4$ , 85 %), both of analytical grade, were used as reagents for the preparation. One liter of an aqueous suspension of  $\text{H}_3\text{PO}_4$  (0.6 M) was slowly added drop by drop to one liter of an aqueous suspension of  $\text{Ca}(\text{OH})_2$  (1 M) while stirring for 2 h at room temperature (Loo et al. 2008). Concentrated NaOH was added until a final pH of 11 was obtained. The white suspension obtained was washed using deionized water and dried in an oven at 80 °C for 24 h (Mateus et al. 2007). The dried powder was calcinated at 400, 500, 600, 700, 800 °C for 3 h. Zinc-doped hydroxyapatite was prepared by adding  $\text{Zn}(\text{NO}_3)_2 \cdot 6\text{H}_2\text{O}$  to the solution. Four samples of hydroxyapatite with zinc concentration of 2, 3, 4, 5 wt% were synthesized (Jallot et al. 2005).

## Synthesis of titanium dioxide nanoparticles

A 7.4 ml of titanium tetra isopropoxide was added, drop by drop, to 30 ml of 1 M HNO<sub>3</sub> aqueous solution, and then agitated for 2 h to give a transparent sol, in which 2.0 g TiO<sub>2</sub> are contained. The pH of the colloidal solution was adjusted to pH 3, with the addition of 1 M NaOH solution after dilution of the colloid with 100 ml water, resulting in a turbid TiO<sub>2</sub> colloid. The suspension was agitated at room temperature, centrifuged, and then washed with distilled water. The isolated TiO<sub>2</sub> was dried for 1 h at 100 °C in air. The resulting powder was then calcinated at 300, 350, 400, 450 °C for 3 h (Robert and Weber 1999; Manivannan et al. 2008).

Powder XRD (Seifert, JSO-DE BYEFLEX 2002, Germany) was utilized to identify the crystalline phase composition. The morphology and crystal structure of the product were observed by TEM. The instrument was JEOL 2000F<sub>x</sub>-II operated at 200 kV, High Resolution, analytical TEM with a W-source and a point-point resolution of 2 Å.

## Cell line and culture

Human hepatocellular carcinoma cells HepG2 (GDC055) were obtained from the National Centre for Cell Sciences, Pune (NCCS), India. The cells were maintained in RPMI-1640 supplemented with 10 % fetal bovine serum (FBS), penicillin (100 U/ml), and streptomycin (100 µg/ml) in a humidified atmosphere of 50 µg/ml CO<sub>2</sub> at 37 °C.

## Reagents

RPMI-1640 was purchased from GIBCO/BRL Invitrogen (Caithersburg, MD, USA). FBS was purchased from Gibco Laboratories. Trypsin, methylthiazolyl diphenyl-tetrazolium bromide (MTT), and dimethyl sulfoxide (DMSO) were purchased from SISCO Research Laboratory Chemicals, Mumbai. All other chemicals and reagents were obtained from Sigma-Aldrich, USA.

## In vitro assay for Cytotoxicity activity (MTT assay)

The cytotoxicity of samples on HepG2 cells was determined by the MTT assay (Mosmann 1983). Cells

(1 × 10<sup>5</sup>/well) were plated in 100 µl of medium/well in 24-well plates (Hi media chemicals Ltd, Mumbai, India). After 48 h incubation the cell reaches the confluence. Then, cells were incubated in the presence of various concentrations of the samples in 0.1 % DMSO for 48 h at 37 °C. After removal of the sample solution and washing with phosphate-buffered saline (pH 7.4), 200 µl/well (5 mg/ml) of 0.5 % 3-(4, 5-dimethyl-2-thiazolyl)-2,5-diphenyl-tetrazolium bromide cells (MTT) phosphate- buffered saline solution was added. After 4 h incubation, 0.04 M HCl/isopropanol were added. Viable cells were determined by the absorbance at 570 nm with reference at 655 nm. Measurements were performed, and the concentration required for 50 % inhibition of viability (IC<sub>50</sub>) was determined graphically. The absorbance at 570 nm was measured with a UV spectrophotometer using wells without sample containing cells as blanks. The effect of the samples on the proliferation of human liver cancer cells (HepG2) was expressed as the % cell viability, using the following formula:

$$\% \text{ cell viability} = \left( \frac{A_{570} \text{ of treated cells}}{A_{570} \text{ of control cells}} \right) \times 100\% \quad (2)$$

## Statistical analysis

Statistical analysis was performed on Software Statistica 6.0. Significant difference between two groups was evaluated by one way analysis of variance (ANOVA) and the level of significance was set as  $P < 0.05$  or  $P < 0.01$  (Zar 1996).

## DNA fragmentation

After treatment with 10 nm (49.02 µg ml<sup>-1</sup>) and 14 nm (37.58 µg ml<sup>-1</sup>) of HAp NPs, 23 nm (15.47 µg ml<sup>-1</sup>) and 27 nm (24.53 µg ml<sup>-1</sup>) of Zn doped HAp and 3 nm (26.77 µg ml<sup>-1</sup>) of TiO<sub>2</sub> nanoparticles for 24 h, human hepatoma cells (HepG2) were collected, washed with PBS, and lysed with a solution containing 10 mmol l<sup>-1</sup> Tris-HCl pH 7.4, 10 mmol l<sup>-1</sup> EDTA, and 0.5 % Triton X-100. The lysates were incubated with 200 mg ml<sup>-1</sup> RNase A (Sigma Aldrich Co, USA) for 1 h followed by 200 mg ml<sup>-1</sup> proteinase K (GIBCO) for 1 h at 37 °C. These samples were then extracted with phenol/chloroform/isoamyl alcohol (25:24:1, v/v/v)

followed by chloroform. DNA was precipitated in two volumes of ethanol in the presence of  $0.3 \text{ mol l}^{-1}$  sodium acetate. The DNA samples thus obtained were run on 1.5 % agarose gel at 50 V and visualized by ethidium bromide staining under UV light (Qi et al. 2005).

### Flow cytometry analysis

HepG2 cells ( $2 \times 10^5$  cells/well) were cultured in 60-mm Petri dishes and incubated for 48 h. The cells were then harvested, washed with phosphate-buffered saline (PBS), then resuspended in 200  $\mu\text{l}$  of PBS, and fixed in 800  $\mu\text{l}$  of ice-cold 100 % ethanol at 4 °C. After being left to stand overnight, the cell pellets were collected by centrifugation, resuspended in 1 ml of hypotonic buffer (0.5 % Triton X-100 in PBS and 0.5 l g/ml RNase), and incubated at 37 °C for 30 min. Next, 1 ml of propidium iodide solution (50  $\mu\text{g/ml}$ ) was added, and the mixture was allowed to stand on ice for 30 min. Fluorescence emitted from the propidium iodide–DNA complex was quantitated after excitation of the fluorescent dye by FACScan cytometry (FACS CANTO II, BD BioSciences, Bangalore).

## Results and Discussion

### Nanoparticle characterization

Figure 1a shows the XRD pattern of hydroxyapatite nanoparticles annealed at different temperature. It shows the formation of single phase hydroxyapatite and the spectrum matches with the JCPDS values (09-0432). The major peaks indicate the crystalline form. The “a” and “c” value of hydroxyapatite nanoparticles are 9.416 Å and 6.886 Å, respectively, which are close to the lattice parameter of stoichiometric hydroxyapatite (powder diffraction file ICDD 09-0432  $a = 9.418 \text{ \AA}$  and  $c = 6.884 \text{ \AA}$ ). At 500 °C the HAp structure started to become visible with peaks corresponding to the (100), (002), (210), (211), (112), (300), (202), and (310) reflections. After heating at 800 °C the samples became more crystalline and other well-defined peaks were also observed. Diffraction peaks of the annealed HAp particles were narrow and well separated as compared to the broad XRD peaks of as-synthesized HAp nanoparticles. It confirms that the sample is of improved crystallinity and increased

crystallite size. The crystalline size of hydroxyapatite nanoparticles can be calculated by Scherrer formula as follows:

$$X_{hkl} = K\lambda / \beta 1/2 \cos \theta \quad (3)$$

where  $X_{hkl}$  is the crystallite size (nm),  $\lambda$  is the wavelength of monochromatic X-ray beam (nm) ( $\lambda = 0.15418 \text{ nm}$  for  $\text{CuK}\alpha$  radiation),  $\beta 1/2$  is the full width at half maximum for the diffraction peak under consideration (rad), “ $\theta$ ” is the diffraction angle (°), and “ $K$ ” is a constant varying with crystal habit and chosen to be 0.9. In the XRD pattern, the (211) peak has the most distinct reflection. So, the mean crystalline size is calculated with the line broadening of the (211) reflection. The crystalline sizes calculated are given in Table 1.

Figure 1b shows the TEM pictures of hydroxyapatite nanoparticles annealed at different temperature. All the HAp samples show spherical morphology of size less than 50 nm with agglomeration. An increase in calcinations temperature gives the system adequate kinetics to permit further growth of the HAp grains. The SAED analyses confirmed the formation of hexagonal structure of HAp, and are in agreement with the XRD results. Whisker morphology remained in the as prepared and samples annealed at 500 and 600 °C. The tip of the crystals annealed at 700 and 800 °C became more rounded off with increase in annealing temperature.

Figure 2 shows the XRD pattern of the zinc-doped hydroxyapatite synthesized with various zinc concentrations. The zinc concentration ( $\text{Zn}/(\text{Ca} + \text{Zn})$ ) is expressed as the weight percentage of zinc. The peak in the Fig. 1b is identical to the XRD pattern of pure hydroxyapatite and no other crystalline phase is detected. As zinc concentration increases, the XRD peak of the samples become broader, indicating lower crystallinity due to the addition of zinc. Table 2 shows the single crystal size and crystallinity of pure hydroxyapatite and zinc-doped hydroxyapatite. As the zinc content increased, both the crystallinity and crystal size decreased gradually.

The zinc-doped hydroxyapatite samples were analyzed by ICP–OES spectroscopy to find out the amount of zinc present in the zinc-doped hydroxyapatite samples. Table 3 gives the amount of zinc in the zinc-doped hydroxyapatite samples. The amount of zinc increases with increase in the amount of zinc added. Raman and XRF analysis of zinc-doped

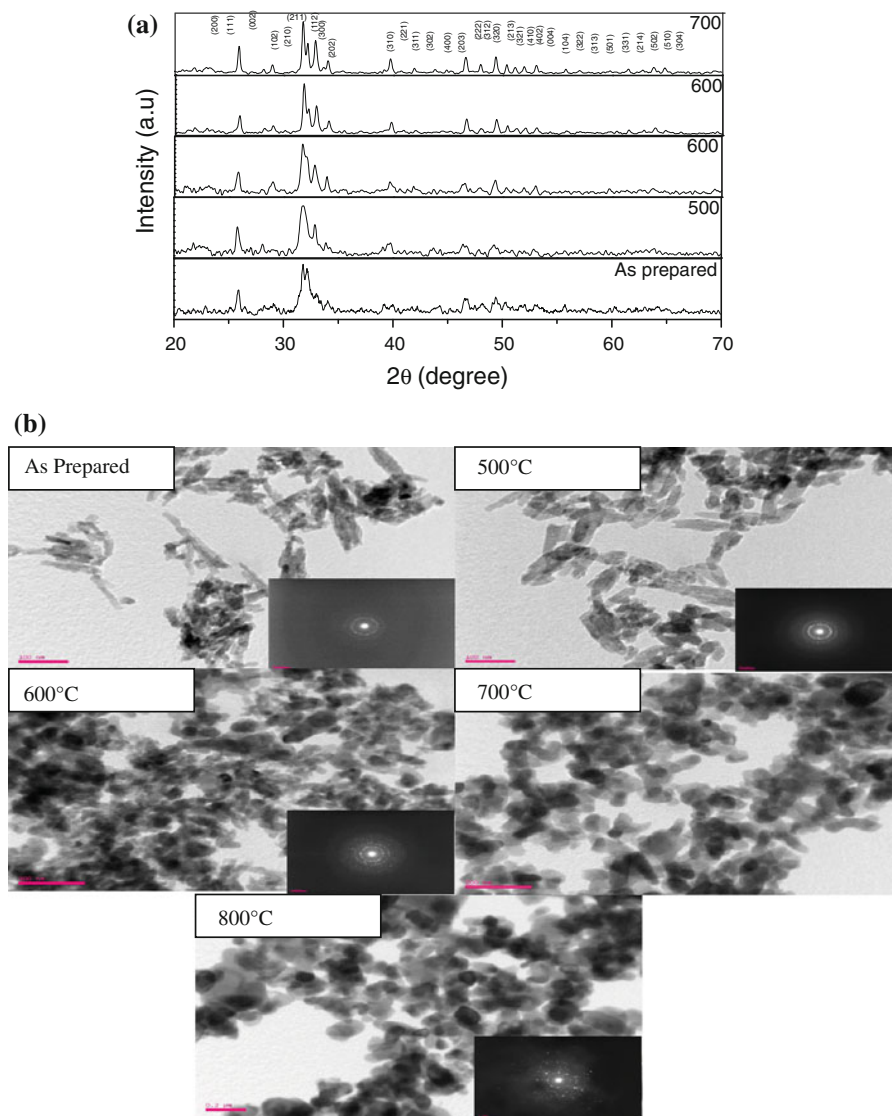


**Fig. 1** **a** XRD pattern of hydroxyapatite nanoparticles annealed for 3 h at different temperature. **b** TEM images of hydroxyapatite nanoparticles annealed at different temperature

**Table 1** Crystal size and crystallinity of hydroxyapatite

S. No	Sample	Line width (211) FWHM (°)	Line width (211) FWHM (rad)	Grain size <i>D</i> (nm)	Crystallinity ( $X_c$ )
1	As synthesized	0.634	0.0136	10	0.034
2	Annealed at 500 °C	0.576	0.0100	14	0.072
3	Annealed at 600 °C	0.344	0.0060	24	0.339
4	Annealed at 700 °C	0.266	0.0046	31	0.734
5	Annealed at 800 °C	0.136	0.0023	60	5.490

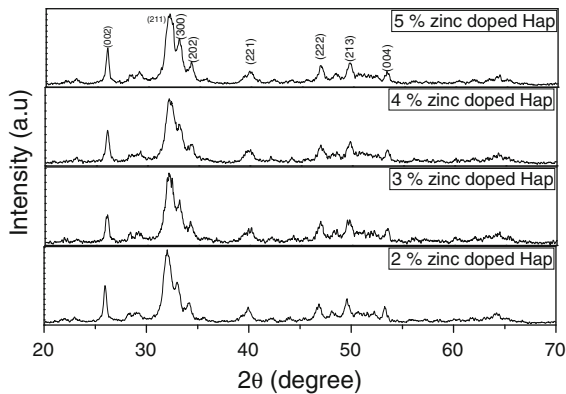


**Fig. 2** XRD of zinc-doped hydroxyapatite nanoparticles

hydroxyapatite were discussed in our previous work (Devanand Venkatasubbu et al. 2011).

Figure 3a shows the XRD patterns for  $\text{TiO}_2$  as a function of annealing. The diffraction peaks corresponds to anatase phase. From 300 to 450 °C only peaks related to anatase structure were evident. Existence of strong crystalline peaks at  $2\theta$  values of 25.20°, 37.80°, 38.57°, 48.04°, 53.890°, 55.06°, 62.11°, 62.68°, and 68.76° corresponding to the crystal planes of (101), (004), (112), (200), (105), (211), (213), (204), and (116) indicates the formation of anatase titanium dioxide (JCPDS card No. 21-1272). As the annealing temperature increases above 300 °C the intensity of (101) peak increases and the line width of the same decrease. This indicates that after annealing the crystallinity of the sample becomes better and the crystallite size increases. The anatase (101) peak was used to determine the grain size by Scherrer formula. The FWHM values and the calculated crystallite sizes, as function of the annealing temperature, are shown in Table 4.

The TEM image of titanium dioxide nanoparticles annealed for 3 h at different temperature are given in

**Table 2** Single crystal size and crystallinity of Zn-doped Hydroxyapatite

Sample	Line width (211) FWHM (°)	Line width (211) FWHM (rad)	Grain size $D$ (nm)	Crystallinity ( $X_c$ )
2 % zinc-doped hydroxyapatite	0.161	0.00280945	50	3.312
3 % zinc-doped hydroxyapatite	0.267	0.00465915	30	0.726
4 % zinc-doped hydroxyapatite	0.292	0.0050954	27	0.555
5 % zinc-doped hydroxyapatite	0.347	0.00605515	23	0.330

**Table 3** ICP-OES values of weight percentage of zinc in zinc-doped hydroxyapatite

S. no	Sample	Zinc concentration (wt%)
1	2 % Zinc-doped hap	0.4990
2	3 % Zinc-doped hap	0.7400
3	4 % Zinc-doped hap	0.9710
4	5 % Zinc-doped hap	1.3740

Fig. 3b. TEM images confirm the formation of spherical particles. As the annealing temperature increases the average particle size (not size of the grain) increases. The increase in the average particle size is very little up to about 450 °C. This agrees well with the results of Siegel et al. (1988). Grains with much agglomeration are clearly observable from the images of low temperature heat treated samples. The particle size of titanium dioxide nanograins varies from 3 to 10 nm as calculated from Scherrer formula. The SAED analyses confirmed the formation of tetragonal structure of titanium dioxide, and are in agreement with the XRD results.

#### Cell viability (MTT assay)

In this study, the exponentially grown human hepatocellular carcinoma cells HepG2 were treated with various concentrations of HAp, Zn-doped HAp, and  $\text{TiO}_2$  nanoparticles ranging from 1.953 to 1.000  $\mu\text{g ml}^{-1}$ , and the cell viability was measured by the MTT assay. The significant inhibition ( $P < 0.05$ ;  $P < 0.01$ ;  $P < 0.001$ ) of cell viability by nanoparticles were clearly observed in a dose dependent manner.

HAp showed size-dependent cytotoxicity against HepG2 cells. The cell viability for HAp nanoparticles of different sizes are given in Fig. 4a. The cell viability

**Fig. 3 a** XRD pattern of titanium dioxide nanoparticles annealed at different temperature (*i*) as Prepared (*ii*) annealed at 300 °C (*iii*) annealed at 350 °C (*iv*) annealed at 400 °C (*v*) annealed at 450 °C. **b** TEM images of titanium dioxide nanoparticles annealed at different temperature

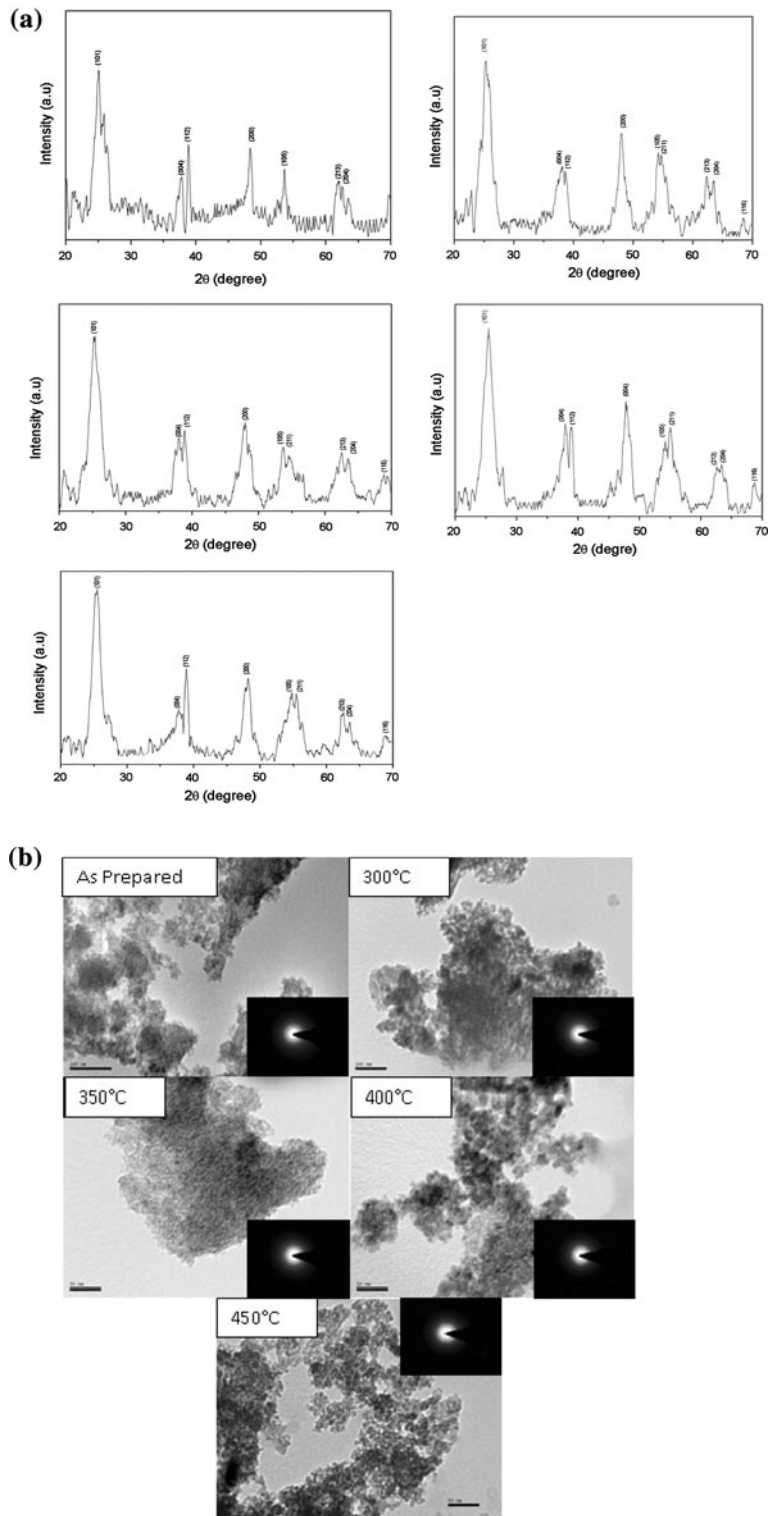
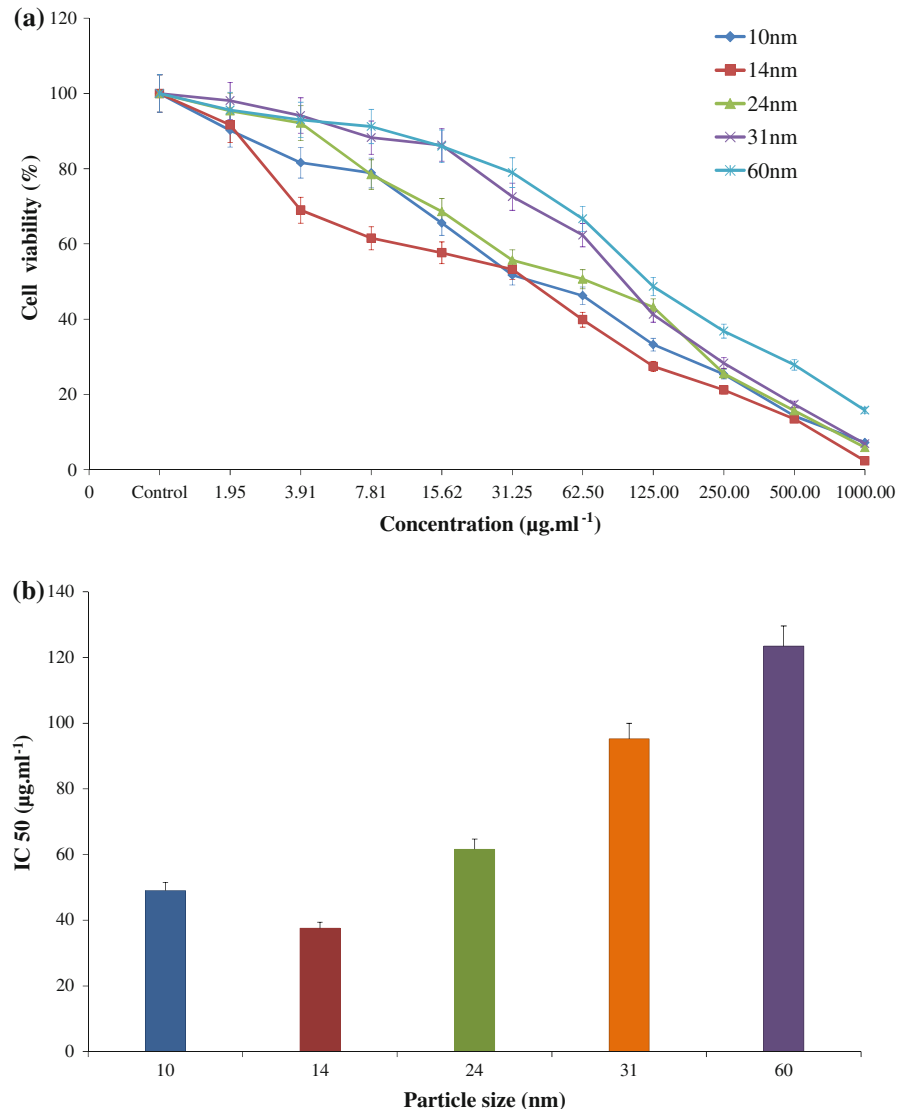


**Table 4** Crystal size and crystallinity of titanium dioxide

S. no	Sample	Line width (101) FWHM (°)	Line width (101) FWHM (rad)	Grain size $D$ (nm)	Crystallinity ( $X_c$ )
1	As Synthesized	2.606	0.0454	3	0.00078
2	Annealed at 300 °C	2.020	0.0352	4	0.00167
3	Annealed at 350 °C	1.627	0.0283	5	0.00320
4	Annealed at 400 °C	1.489	0.0259	6	0.00418
5	Annealed at 450 °C	1.156	0.0145	7	0.00567

**Fig. 4 a** Cytotoxicity effect of hydroxyapatite nanoparticles of different particle size at different concentration versus control. **b** Dependence of the cell viability on hydroxyapatite nanoparticle particle size

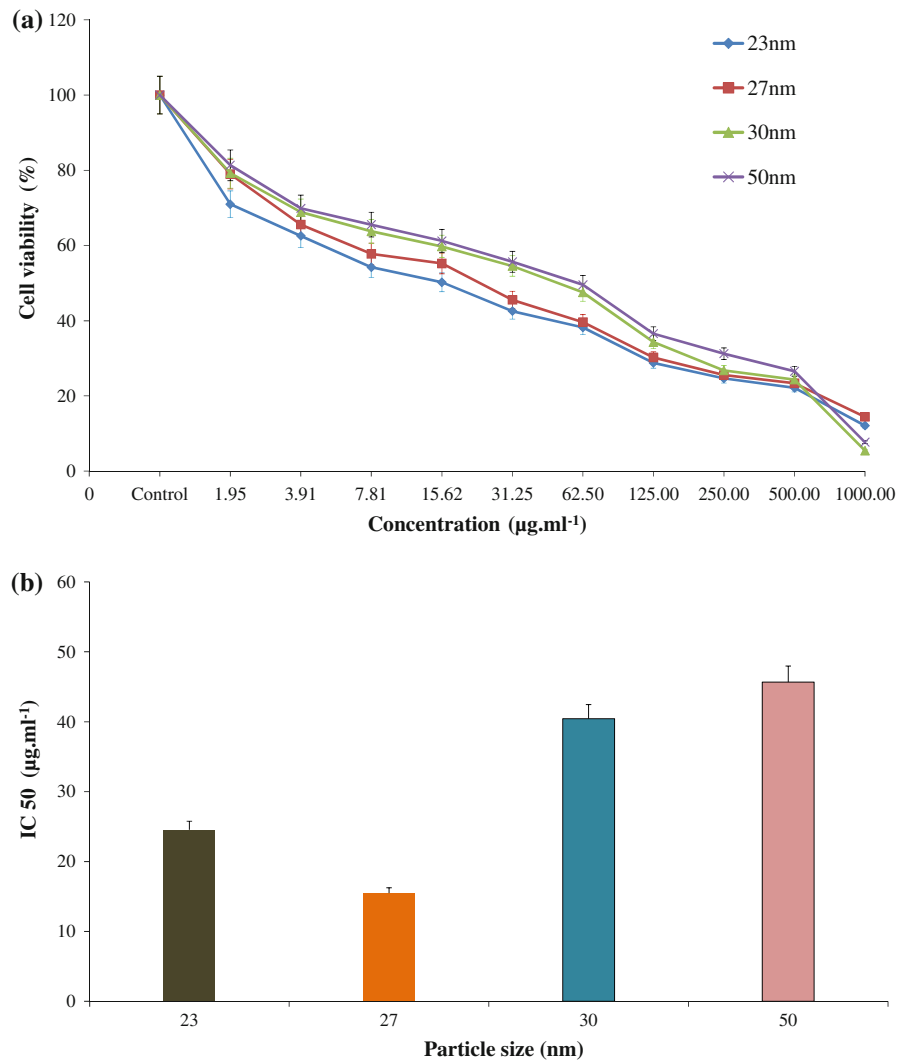


decreases with increase in the concentration of the nanoparticles. As the concentration of HAp nanoparticles is increased from 1.953 to 1.000 µg ml<sup>-1</sup> the cell viability decreased. This is observed in HAp

nanoparticles of different sizes. The variation in IC<sub>50</sub> values as a function of size of nanoparticles is given in the Fig. 4b. The IC<sub>50</sub> value for HAp nanoparticles of size 10 nm is 49.02 µg ml<sup>-1</sup>, 14 nm



**Fig. 5 a** Cytotoxicity effect of zinc-doped hydroxyapatite nanoparticles of different particle size at different concentration versus control. **b** Dependence of the cell viability on zinc-doped hydroxyapatite nanoparticle particle size



is  $37.58 \mu\text{g ml}^{-1}$ , 24 nm is  $61.62 \mu\text{g ml}^{-1}$ , 31 nm is  $95.24 \mu\text{g ml}^{-1}$ , and for 60 nm is  $123.45 \mu\text{g ml}^{-1}$ . When the particle size increases, the  $\text{IC}_{50}$  value also increases. But the  $\text{IC}_{50}$  value for HAp nanoparticles of size 14 nm is lesser than 10 nm size HAp nanoparticles. The cell viability of HepG2 cells significantly decreased after exposure to HAp nanoparticles of sizes 10, 24, 31, and 60 ( $P < 0.01$ ) and ( $P < 0.001$ ) for 14 nm size particle after 48 h. In particular, when the HepG2 cells were treated by HAp nanoparticles of size 14 nm, the loss of cell viability attained as high as 62.42 %. HAp nanoparticles of size 60 nm exerted a weak inhibitory activity in HepG2 cells. This clearly shows that the anticancer activity of HAp

nanoparticles against HepG2 cells was significantly dependent on the particle size.

Zinc-doped HAp also showed size-dependent cytotoxicity against HepG2 cells. Upon increasing the amount of dopant, the amount of zinc in the HAp nanoparticles increases. This leads to the decrease in the particle size. So the particle size of zinc-doped HAp is lesser than the pure HAp. The particle size decreases as the percentage of dopant is increased. The cell viability for zinc-doped HAp nanoparticles of different concentration is given in Fig. 5a. The variation in  $\text{IC}_{50}$  values depending up on the nanoparticle size is given in the Fig. 5b. The  $\text{IC}_{50}$  value for zinc-doped HAp nanoparticles is  $15.47 \mu\text{g ml}^{-1}$  for

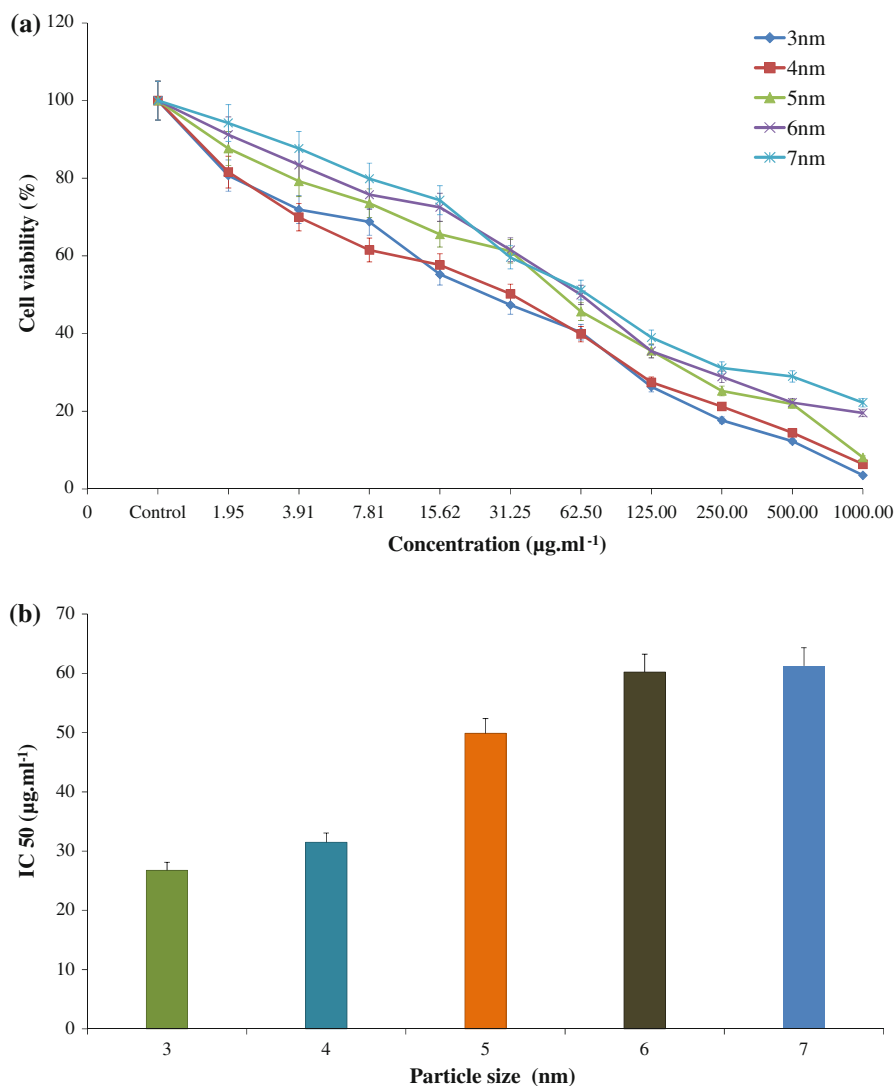


**Fig. 6** **a** Cytotoxicity effect of titanium dioxide nanoparticles of different particle size at different concentration versus control. **b** Dependence of the cell viability on titanium dioxide nanoparticle particle size

23 nm, 24.53 µg ml<sup>-1</sup> for 27 nm, 40.43 µg ml<sup>-1</sup> for 30 nm, and 45.67 µg ml<sup>-1</sup> for 50 nm. With the increase in particle size the IC<sub>50</sub> value increases. The cell viability is significantly decreased after exposure to zinc-doped HAp nanoparticles of sizes 27, 30 ( $P < 0.01$ ) and 23, 50 ( $P < 0.05$ ) for 48 h. In particular, when the cells were treated by zinc-doped HAp nanoparticles of size 23 nm, the loss of cell viability attained as high as 84.53 %. Zinc-doped HAp nanoparticle of size 50 nm has less anticancer activity in HepG2 cells. This implies that the anticancer activity increases with increase in zinc concentration. Zinc-

doped HAp nanoparticles of size 23 nm have high zinc content. The zinc content increases with decreasing particle size. As the concentration of zinc in zinc-doped HAp increases from 0.4990 to 1.3740 wt% the anticancer activity also increases. This clearly shows that the anticancer activity of zinc-doped HAp nanoparticles against HepG2 cells were significantly dependent on the zinc concentration. This implies that the anticancer activity of HAp nanoparticles increases when doped with zinc.

Cell proliferation in response to different concentrations of TiO<sub>2</sub> nanoparticles present in the culture

media was evaluated by the MTT assay. There were slight changes in the cell viability at lower concentrations of TiO<sub>2</sub> nanoparticles, and as the concentration increased, cell viability decreased drastically. In comparison with the control group, cells cultured in medium containing TiO<sub>2</sub> nanoparticles for 48 h showed a decrease in viability. The variation in cell viability with different concentration of TiO<sub>2</sub> is given in Fig. 6a. TiO<sub>2</sub> also showed size-dependent cytotoxicity against HepG2 cells. The IC<sub>50</sub> for TiO<sub>2</sub> nanoparticles of different sizes is given in Fig. 6b. The cell viability significantly decreased after exposure to TiO<sub>2</sub> nanoparticles of sizes 3 nm ( $P < 0.001$ ) and 4, 5, 6, and 7 nm ( $P < 0.01$ ) size particle after 24 h. The IC<sub>50</sub> value for TiO<sub>2</sub> particle of 3 nm is 26.77  $\mu\text{g ml}^{-1}$  and it is 31.48  $\mu\text{g ml}^{-1}$ , 49.88  $\mu\text{g ml}^{-1}$ , 60.23  $\mu\text{g ml}^{-1}$ , and 61.25  $\mu\text{g ml}^{-1}$  for 4, 5, 6, and 7 nm, respectively. The cell viability is very low for 3 nm size particle and it increases with increase in particle size. At 3 nm the loss of cell viability is as high as 68.53 %.

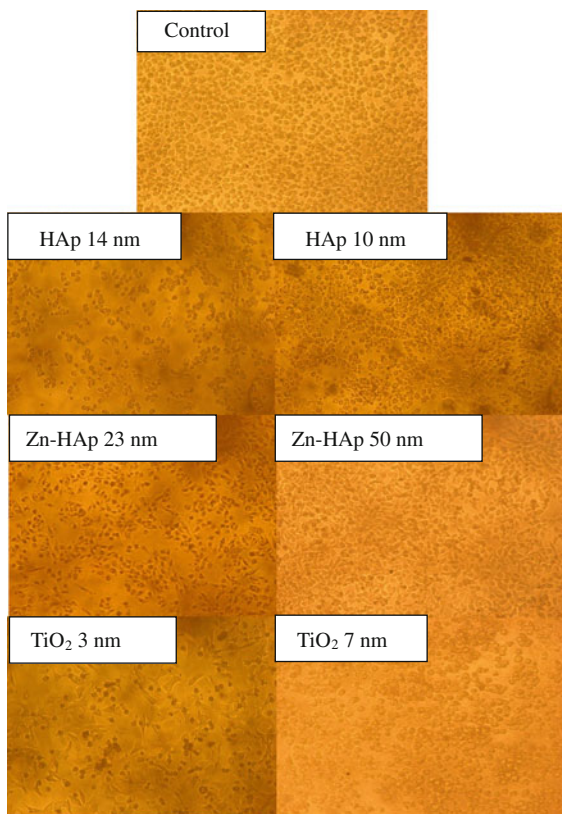


**Fig. 7** Observations of HepG2 cell morphological changes after treated with nanoparticles for 24 h. The cells were observed by optic microscope directly

The experiments with MTT assay after 48 h showed significantly lower cell proliferation compared to control as shown in Fig. 7. In 14 nm HAp nanoparticles the value is less than those treated with 10 nm HAp NPs. For Zn doped HAp NPs, MTT assay showed minimum cell proliferation in 23 nm Zn doped HAp NPs compared to 50 nm. The maximum reduction in cell proliferation was observed at 3 nm compared to 7 nm TiO<sub>2</sub> NPs. Taken together, these results demonstrate that maximum intake of NPs was observed in 14 nm HAp, 23 nm Zn doped HAp NPs, and 3 nm TiO<sub>2</sub> NPs.

The impact of particle size on cellular uptake and ensuing functional impact is well known. The HAp nanoparticles used in this study ranges between 10 and 60 nm. It is obtained by wet chemical method and modulating the calcinations temperature in the range 500–800 °C. Results obtained showed that NPs induced significant growth inhibition and the strength of the anti-proliferative effect was in the order of 14 nm > 10 nm > 24 nm > 31 nm > 60 nm for HAp NPs. Nanoparticles interact with the biomolecules on the surface or within the cells (Jiang et al. 2008). So cellular trafficking plays an important role in the size dependents of HAp nanoparticles. Particle size also plays an important role in determining the nuclear penetration of HAp nanoparticles. Due to passive mechanism nanoparticles of different size have different biodistribution. The cellular uptake of nanoparticle is a two step process. First, the uptake of the nanoparticles from surface of the cell to cytoplasm and then cellular trafficking of the nanoparticle. Nanoparticles of size ~50 nm are readily taken up by the cells than the particles of other sizes by endocytotic mechanism (Bansal and Chaudhary 2005). Particles smaller than 50 nm tend to form cluster and aggregate during uptake. This is due to higher surface curvature of smaller nanoparticles which restricts the binding and the mutual adsorption between the nanoparticles and cells. For nanoparticles larger than 50 nm, the slower receptor diffusion rate is the reason for fewer nanoparticles taken by cells (Chithrani and Chan 2007). In our study we found that more than other sizes, more HAp nanoparticles of size 14 nm had been taken up by the cells.

The increase in anticancer activity of zinc-doped hydroxyapatite is due to the presence of Zn<sup>2+</sup> ions in hydroxyapatite. Ultrasonic radiation causes lipid peroxidation in the liposomal membrane. Three reaction

products of lipid peroxidation are conjugated dienes, lipid hydroperoxides, and malondialdehydes. They were detected in the ultrasound-exposed liposomal membrane. The reaction products are produced at different stages of a lipid peroxidation chain reaction mediated by free radicals. Lipid peroxidation is inhibited by free radical scavengers. The ultrasound-induced lipid peroxidation thus appears to be the result of a chain reaction involving oxygen and mediated by free radicals (Chatterjee and Agarwal 1988; Jana et al. 1990; Kanagalakshmi et al. 2010). Potential redox properties of glycine- $Zn^+/Zn^{2+}$  in a biological system have been described by Ai et al. (2003) and it is also possible that sequential oxidation–reduction reactions may occur to produce reactive species such as hydrogen peroxide ( $H_2O_2$ ) and hydroxyl radical ( $OH\cdot$ ) (Ai et al. 2003). The enhanced anticancer activity in zinc-doped Hap may be due to the reactive oxygen species (ROS) production. The reaction between the  $Zn^{2+}$  and cell envelope components and between the  $Zn^{2+}$  ions and components in the interior of the cell may also be reasons for higher anticancer activity of zinc-doped HAp.

$TiO_2$  particle-mediated anticancer activity is due to particle-cell interactions. It is due to the surface properties of the  $TiO_2$  particles.  $TiO_2$  particles have a net negative charge (at pH 7) and also bind preferentially to amino acids containing  $-OH$ ,  $-NH$ , and  $-NH_2$  in their side chains. These observations indicate that  $TiO_2$  particles may react with cell membrane proteins and contribute to cell particle interaction (Tran et al. 2006).

Ceramic nanoparticles are used in photodynamic therapy for cancer treatment (Subramani et al. 2009). The metal ions released from metal oxide nanoparticles are involved in the cytotoxicity of metal oxide nanoparticles. The release of  $Ca^{2+}$ ,  $Zn^{2+}$  ions from pure hydroxyapatite and zinc-doped hydroxyapatite are responsible for the cytotoxicity. The electrostatic interaction between the cell membrane and the nanoparticle is the main reason for attachment (Hosseinkhani and Tabata 2006). The cytotoxicity of  $TiO_2$  is mainly due to protein adsorption. The adsorption of the components of the culture media onto the metal oxide nanoparticles induces a starvation state and subsequent enervation of cells in vitro. The coating of the metal oxide nanoparticles with proteins may change their biological activities. Protein adsorption to metal oxide depends on the surface charge of the

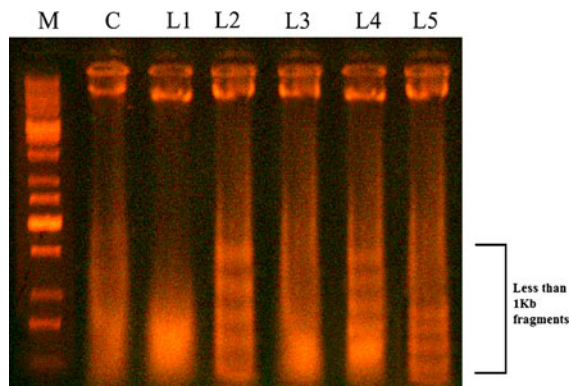


**Fig. 8** Agarose gel electrophoretic analysis of DNA isolated from human hepatoma cells (HepG2) incubated with different concentrations of NPs for 24 h. C control, M marker. L1—10 nm HAp NPs ( $49.02 \mu\text{g ml}^{-1}$ ), L2—14 nm HAp NPs ( $37.58 \mu\text{g ml}^{-1}$ ), L3—23 nm Zn doped HAp NPs ( $15.47 \mu\text{g ml}^{-1}$ ), L4—27 nm Zn doped HAp NPs ( $24.53 \mu\text{g ml}^{-1}$ ), L5—3 nm  $TiO_2$  NPs ( $26.77 \mu\text{g ml}^{-1}$ )

protein and the particle. Thus, the isoelectric point of the metal oxide is important for protein adsorption (Horie et al. 2009).

#### DNA fragmentation

The DNA damaging effect of HAp, Zn-doped HAp, and  $TiO_2$  nanoparticles in HepG2 were evaluated using DNA fragmentation studies (Fig. 8). The concentrations of NPs used in this study were based on the results of  $IC_{50}$  values obtained from cytotoxicity assay. Control DNA, 10 nm HAp NPs, and 14 nm HAp NPs, 23 and 27 nm Zn-doped HAp NPs, and 3 nm  $TiO_2$  NPs were examined for DNA fragmentation. Control, 10 nm HAp NPs and 23 nm Zn-doped HAp NPs showed the presence of undamaged genomic DNA represented by a thick band on the agarose gel, the highest extent of DNA damage was observed for 14 nm HAp NPs, 27 nm Zn-doped HAp NPs, and 3 nm  $TiO_2$  NPs. At 3 nm of  $TiO_2$  and 14 nm of HAp NPs, large number of fragments, less than 1 kb was observed when compared to control group.

The nanoparticles trigger the changes of expression of the apoptotic proteins, and thereby induce the apoptosis and cytotoxicity only within the cell nucleus of the HepG2 cells. 14 nm HAp NPs with the most efficient cellular uptake and nuclear trafficking led to the greatest changes of the apoptotic proteins and the strongest anti-tumor activity, and apoptosis in HepG2

cells. For 60 nm HAp NPs, although taken up by HepG2 cells, they cannot penetrate into cellular nucleus. Thus, the weakest cytotoxicity and apoptosis induction were observed. During cellular trafficking of the nanoparticles needs to cross the double nuclear membrane, which separates the nucleoplasm from the rest of the cell. This nuclear membrane contains specialized channels called nuclear pore complexes (NPCs), through which nuclear import and export occur. The nanoparticles should be smaller than the NPCs to enter nucleus. The sizes of NPs vary from 20 to 50 nm, and it varies with cell type (Wente 2000). HAp nanoparticles are not uptaken by hepatocarcinoma cells by simple diffusion, or membrane protein transportation, or pinocytosis because they are not micromolecules or materials with <10 nm diameter, or dissolved matter. Hepatocarcinoma cells are not specialized cells like neutrophils or macrophages practicing phagocytosis. Phagocytosis is not the mechanism used by the hepatocarcinoma cells to intake HAp nanoparticles. The uptake of HAp nanoparticle into the hepatoma carcinoma cells were by the caveolae is well established by Yin et al. (2010). The size of the caveolae plays an important role in the uptake of the substance. The results of present study suggest TiO<sub>2</sub> nanoparticles generate large amount of hydroxyl free radical thereby leading to DNA damage (Reeves et al. 2007). The HAp particles, only within the cell nucleus of the HepG2 cells, can trigger the changes of expression of the apoptotic proteins, and thereby induce the apoptosis and cytotoxicity. Thus the cytotoxic and genotoxic mechanism of HAp, Zn-doped HAp, and TiO<sub>2</sub> NPs is related to their membrane penetration and apoptosis activity.

Several studies have indicated that the phenomenon of cellular uptake is of crucial importance in governing a range of cellular behaviors including cell growth, apoptosis, adhesion, migration, differentiation, survival, and tissue organization (Absolom et al. 1987). Current studies in this area have demonstrated that physicochemical properties of NPs, including particle size, chemical composition, and surface chemistry, can affect NPs nonspecific uptake ability. NP size and concentration-dependent effects are important. Metal oxide nanoparticles spontaneously produce ROS based on material composition and surface characteristics. But other nanomaterials produce ROS only in the presence of selected cell systems. When the production of ROS is higher and the cellular

antioxidant defense system is not capable of controlling them, oxidative stress occurs. This results in the damage of cellular components like lipids, proteins, and DNA (Lovric et al. 2005; Xia et al. 2006; Long et al. 2006). Lipid peroxide, produced when fatty acid is oxidized, initiates a chain reaction resulting in disruption of plasma and organelle membranes and subsequent cell death. HAp, zinc-doped HAp, and TiO<sub>2</sub> start the apoptosis process with fragmentation of DNA (Fig. 9). Apoptosis is the programmed death of cells by fragmentation of DNA, cell shrinkage, followed by cell fragmentation and formation of membrane vesicles called apoptosis bodies. Dysregulation of apoptosis is linked to the development of most cancers. Thus, an induction of apoptosis in cancer cells is considered as a new focus in the discovery of anticancer drugs. DNA cleavage at the internucleosomal linker sites yielding DNA fragments is regarded as a biochemical hallmark of apoptosis. Primary mechanism of these nanoparticles and anti-cancer activity might proceed by inducing the generation of ROS, which then were responsible for the induction of apoptosis.

#### Flow cytometry analysis

Cell cycle arrest analysis for HAp, zinc-doped HAp, and TiO<sub>2</sub> nanoparticles are given in Fig. 9. When HepG2 cells were treated with various concentrations of HAp for 24 h (Fig. 9(i)), G<sub>2</sub>/M phase arrest was observed in a concentration-dependent manner. When the concentration of HAp nanoparticles added was increased from 15.625 to 31.25 µg/ml an increase in the percentage of cells in the G<sub>2</sub>/M phase from 25.67 to 45.17 %, respectively, is observed compared to that of control (14.56 %). When HepG2 cells were treated with various concentrations of zinc-doped HAp for 24 h (Fig. 9(ii)), S phase arrest was observed in a concentration-dependent manner. When the concentration of zinc-doped HAp nanoparticles added was increased from 3.906, 7.812, and 15.625 µg/ml an increase in the percentage of cells in the S phase from 27.89, 46.78, and 78.90 %, respectively, is observed compared to that of control (5.67 %). When HepG2 cells were treated with various concentrations of TiO<sub>2</sub> for 24 h (Fig. 9(iii)), a significant increase in sub-G<sub>1</sub> population was observed. The percentage of cells increases from 31.29 to 59.11 % for 31.25 and

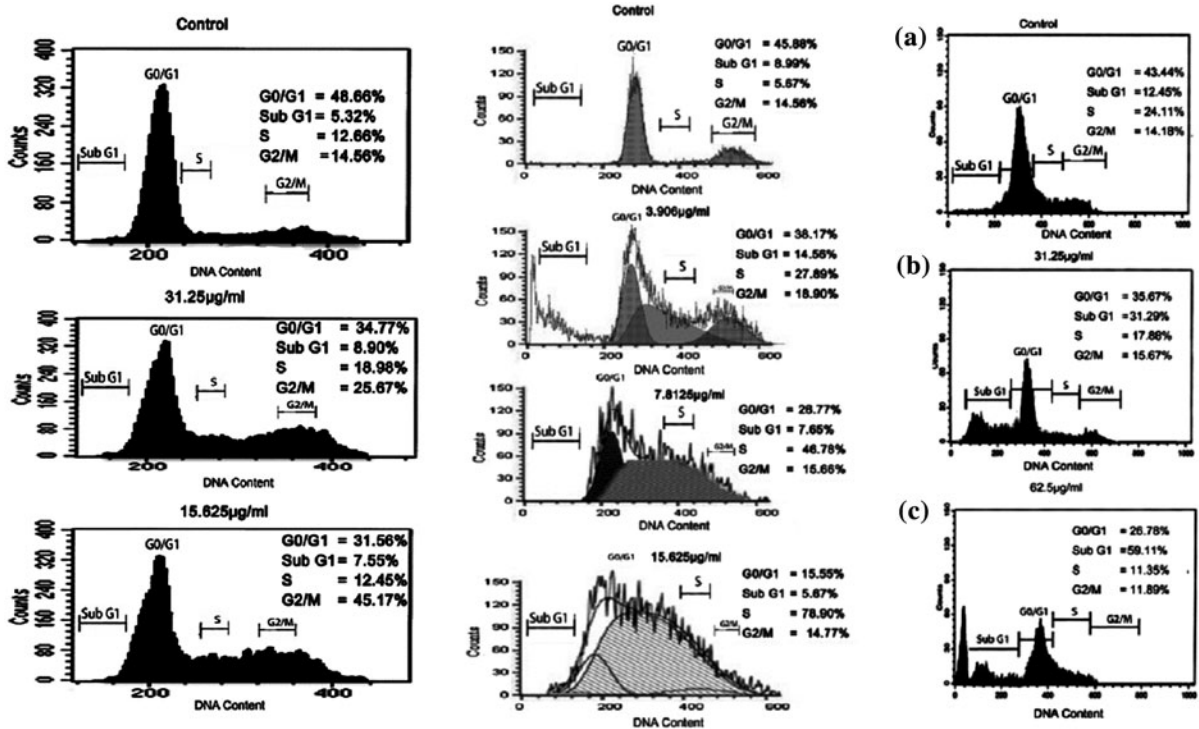


**Fig. 9** Fluorescence activated cell sorting (FACS) analysis revealed (i) The HepG2 cells with HAp after 48 h. Maximum percentage inhibition was at G0/G1 phase in 15.625 μg/ml HAp. (ii) The Hep G2 cells with Zn doped HAp after 48 h. Maximum

percentage inhibition was at Sub G1 phase in 62.5 μg/ml Zn doped HAp. (iii) The Hep G2 cells with TiO<sub>2</sub> after 48 h. Maximum percentage inhibition was at S phase in 15.625 μg/ml TiO<sub>2</sub>

62.50 μg/ml, respectively compared to that of control (12.45 %).

Apoptosis is programmed cell death which is a normal physiologic process that occurs during embryonic development and in the ongoing process of tissue homeostasis in the adult animals. Any dysregulation of apoptosis can result in abnormality, disease, and death (Wilson et al. 1998). Cancer is a result of the dysregulation of apoptosis as well as uncontrolled cell proliferation (Han et al. 1999). Recently, inducers of apoptosis have been used in cancer therapy. Activation of apoptosis pathways is a key mechanism by which cytotoxic drugs kill tumor cells. It is now considered as an important method of assessment for the clinical effectiveness of many anti-tumor drugs.

HAp inhibited HepG2 cells growth via arresting cell cycle at G2/M phase and inducing apoptosis. Cyclin A, cyclin B1, Cdc2, Cdc 25C, and p21 proteins have been reported to influence G2/M transition in cell cycle (Molinari 2000; Coqueret 2003). CDKs play an

important role in cell cycle progression and have been considered as drug targets (Molinari 2000). Among these CDKs, Cdc2 (CDK1) activation requires phosphorylation on Thr-161 and dephosphorylation on Thr-14 and Tyr-15 (Millar et al. 1997; Honda et al. 1993). Activated Cdc2 interacts with cyclin A and/or cyclin B1 to form an active heterodimer to participate in the progression from G2 to M phase. Cdc25C is required for entry into mitosis and is believed to be the major phosphatase that dephosphorylates Thr-14 and Tyr-15 of Cdc2 (Millar et al. 1997). Therefore, G2/M phase arrest by PMF might be due to the decrease of Cdc2 complex activity, which may be mediated through downregulation of Cdc25C protein to inhibit dephosphorylation of Cdc2 at Thr-14 and Tyr-15 and inhibition of cyclin A expression to decrease the formation of cyclin A/Cdc2 complex. p21 has been found to contribute to arrest cell cycle at G2 phase via blocking the activating phosphorylation of Cdc2 on Thr-161 (Smits et al. 2000). Upregulation of p21

protein may be involved in PMF-mediated G2/M arrest in HepG2 cells via blocking phosphorylation of Cdc2 at Thr161.

Zinc-doped hydroxyapatite nanoparticles induces S phases arrest in HepG2 cells. Cyclin-dependent kinase inhibitors (CDKIs) play a key role in controlling cell cycle progression by negatively regulating the Cdk activities at an appropriate point in the cell cycle (Coqueret 2003). In vertebrate cells, the S phase arrest is triggered by regulation of cyclin A–Cdk2 complex and Cdk1, which promote the breakdown of the nuclear membrane, chromatin condensation, and microtubule spindle formation (King et al. 1994). This may be the mechanism behind the S phase arrest by zinc-doped hydroxyapatite nanoparticles and the presence of zinc may play a vital role.

TiO<sub>2</sub> treated cells has shown sub G<sub>1</sub> phase arrest. Cells undergoing apoptosis were found to have an elevation of cytochrome c in the cytosol, with a corresponding decrease in the mitochondria (Yang et al. 1997). After the release of mitochondrial cytochrome c, the cysteine protease 32 kDa proenzyme CPP32, a caspase 3, is activated by proteolytic cleavage into an active heterodimer (Nicholson et al. 1995). Activated caspase 3 is responsible for the proteolytic degradation of poly (ADP-ribose) polymerase, which occurs at the onset of apoptosis (Lazebnik et al. 1994; Tewari et al. 1995). Internucleosomal DNA fragmentation is not essential for apoptotic cell death. Some necrotic cell death is accompanied by inter nucleosomal DNA fragmentation, suggesting the possibility that this fragmentation may not be sufficient as an indicator of apoptotic cell death (Cohen et al. 1992; Schulze-Osthoff et al. 1994). The central mechanism of apoptosis is evolutionarily conserved, and that caspase activation is an essential step in this complex apoptotic pathway (Thornberry and Lazebnik 1998). The Bcl-2 family plays an important regulatory role in apoptosis, either as activator (Bax) or as inhibitor (Bcl-2) (Rao and White 1997; Green and Reed 1998; Adams and Cory 1998). It has also been demonstrated that the gene products of Bcl-2 and Bax play important roles in apoptotic cell death (Oltvai et al. 1993; Jacobson and Raff 1995; Jacobson et al. 1994). Of the Bcl-2 family members, the Bcl-2 and Bax protein ratio has been recognized as a key factor in regulation of the apoptotic process (Rao and White 1997; Green and Reed 1998; Adams and Cory 1998). TiO<sub>2</sub> may induce apoptosis and sub -G1

arrest by inhibiting the protein expression of anti-apoptosis proteins, survivin, and Bcl-xL. It may disturb the Bcl-2/Bax ratio and, therefore, lead to apoptosis. Many of the agents that induce apoptosis are oxidants or stimulators of cellular oxidative metabolism, while many inhibitors of apoptosis show antioxidant activity (Buttke and Sandstrom 1994). Indeed, factors for oxidative stress, such as ROS production (Coyle and Puttfarcken 1993; Loo et al. 1993; Albrecht et al. 1994; Garcia-Ruiz et al. 1997; Kruman et al. 1997), lipid peroxidation (Hockenbery et al. 1993), downregulation of the antioxidant defenses characterized by reduced glutathione levels (Marchetti et al. 1996), and reduced transcription of superoxide dismutase, catalase, and thioredoxin, have been observed in some apoptotic processes (Briehl and Baker 1996). Moreover, ROS can also play an important role in apoptosis by regulating the activity of certain enzymes involved in the cell death pathway (Coyle and Puttfarcken 1993; Loo et al. 1993; Albrecht et al. 1994; Albrecht et al. 1994; Garcia-Ruiz et al. 1997; Kruman et al. 1997). All these factors point to a significant role for intracellular oxidative metabolites in the regulation of apoptosis. ROS production was probably the cause of this apoptotic cell death.

## Conclusion

In this study, the structural and functional effect of HAp, zinc-doped HAp, and TiO<sub>2</sub> on hepatocellular carcinoma cells in vitro was investigated. We have demonstrated that the size of nanoparticles had obvious effect on the anti proliferation activity. HAp, zinc-doped HAp, and TiO<sub>2</sub> particles have the potential to treat cancer. In HAp, 14 nm size HAp nanoparticle have higher activity. In zinc-doped HAp, 23 nm size particle have higher activity and in TiO<sub>2</sub> 3 nm size particles have high activity. The presence of zinc in zinc-doped HAp is the reason for higher anticancer activity. The cytotoxic and genotoxic mechanism of HAp, Zn-doped HAp, and TiO<sub>2</sub> NPs is related to their membrane penetration and apoptosis activity. Cell cycle arrest analysis for HAp, zinc-doped HAp, and TiO<sub>2</sub> nano particles revealed the influence of HAp, zinc-doped HAp, and titanium dioxide nanoparticles on the apoptosis of HepG2 cells. Our future work is to modify the surface of these

nanoparticles and utilize them as drug carriers in targeted drug delivery systems.

**Acknowledgments** Prof. S. Ramasamy, CSIR Emeritus Scientist and Mr. G. Devanand Venkatasubbu, CSIR-SRF, Dr. L. Palanikumar, CSIR-RA acknowledge the financial support given to them to carry out this study under the CSIR Emeritus Scientist Scheme number 21(0714)/08/EMR-II dated 28-04-2008. The authors are grateful to Dr. (Mrs). V. Meenakumari Ph.D, Professor, Department of English, A.P.A college for women, Palani, an autonomous college of Mother Theresa University, for making English correction in the manuscript.

## References

- Absolom DR, Zingg W, Neumann AW (1987) Protein adsorption to polymer particles—role of surface-properties. *J Biomed Mater Res* 21:161–171
- Adams JM, Cory S (1998) The Bcl-2 protein family: arbiters of cell survival. *Science* 281:1322–1326
- Ai H, Bu Y, Han K (2003) Glycine-Zn<sup>+</sup>/Zn<sup>2+</sup> and their hydrates: on the number of water molecules necessary to stabilize the zwitterionic glycine-Zn<sup>+</sup>/Zn<sup>2+</sup> over the nonzwitterionic ones. *J Chem Phys* 118:10973–10985
- Albrecht H, Tschopp J, Jongeneel CV (1994) Bcl-2 protects from oxidative damage and apoptotic cell death without interfering with activation of NF-kappa B by TNF. *Fed Eur Biochem Soc Lett* 351:45–48
- Bansal SRV, Chaudhary M (2005) Biocompatibility of gold nanoparticles and their endocytotic fate inside the cellular compartment: a microscopic overview. *Langmuir* 21:10644–10654
- Bohner M (2001) Physical and chemical aspects of calcium phosphates used in spinal surgery. *Eur Spine J* 10:114–121
- Briehl MM, Baker AF (1996) Modulation of the antioxidant defense as a factor in apoptosis. *Cell Death Differ* 3:63–70
- Buttke TM, Sandstrom PA (1994) Oxidative stress as a mediator of apoptosis. *Immunol Today* 15:7–10
- Chatterjee SN, Agarwal S (1988) Liposomes as membrane model for study of lipid peroxidation. *Free Radical Biol Med* 4:51–72
- Chithrani BD, Chan WCW (2007) Elucidating the mechanism of cellular uptake and removal of protein-coated gold nanoparticles of different sizes and shapes. *Nano Lett* 7:1542–1550
- Cohen GM, Sun XM, Snowden RT, Dinsdale D, Skilleter DN (1992) Key morphological features of apoptosis may occur in the absence of internucleosomal DNA fragmentation. *Biochem J* 286:331–334
- Coqueret O (2003) New roles for p21 and p27 cell-cycle inhibitors: a function for each cell compartment? *Trends Cell Biol* 13:65–70
- Coyle JT, Puttfarcken P (1993) Oxidative stress, glutamate, and neurodegenerative disorders. *Science* 262:689–695
- de Lima IR, Coasta AM, Bastos IN (2006) Development and characterization of 5% mol Zn bioceramic in granular form. *Mater Res* 9:399–403
- Devanand Venkatasubbu G, Ramasamy S, Ramakrishnan V, Kumar J (2011) Nanocrystalline hydroxyapatite and zinc doped hydroxyapatite as carrier material for controlled delivery of ciprofloxacin. *Biotechnology* 1:173–186
- Garcia-Ruiz C, Colell A, Mari M, Morales A, Fernandez-Checa JC (1997) Direct effect of ceramide on the mitochondrial electron transport chain leads to generation of reactive oxygen species. Role of mitochondrial glutathione. *J Biol Chem* 272:11369–11377
- Green DR, Reed JC (1998) Mitochondria and apoptosis. *Science* 281:1309–1312
- Han X, Wang F, Yao W, Xing H, Weng D, Song X et al (1999) Subcellular distribution and redistribution of BCL-2 family proteins in human leukemia cells undergoing apoptosis. *Blood* 93:2353–2359
- Harhaji L, Isakovic A, Raicevic N, Markovic Z, Todorovic-Markovic B, Nikolic N et al (2007) Multiple mechanisms underlying the anticancer action of nanocrystalline fullerene. *Eur J Pharmacol* 568:89–98
- Hockenbery DM, Oltvai ZN, Yin XM, Millman CL, Korsmeyer SJ (1993) Bcl-2 functions in an antioxidant pathway to prevent apoptosis. *Cell* 75:241–251
- Honda R, Ohba Y, Nagata A, Okayama H, Yasuda H (1993) Dephosphorylation of human p34cdc2 kinase on both Thr-14 and Tyr-15 by human cdc25B phosphatase. *FEBS Lett* 318:331–334
- Horie M, Nishio K, Fujita K, Kato H, Nakamura A, Kinugasa S et al (2009) Ultrafine NiO particles induce cytotoxicity in vitro by cellular uptake and subsequent Ni(II) release. *Chem Res Toxicol* 22:1415–1426
- Hosseinkhani H (2006) DNA nanoparticles for gene delivery to cells and tissue. *Int J Nanotechnol* 3:416–461
- Hosseinkhani H, Tabata Y (2006) Self assembly of DNA nanoparticles with polycations for the delivery of genetic materials into cells. *J Nanosci Nanotechnol* 8:2320–2328
- Hosseinkhani M, Hosseinkhani H, Chen Y-R, Subramani K (2011) In vitro physicochemical evaluation of DNA nanoparticles. *Int J Nanotechnol* 8:736–748
- Jacobson MD, Raff MC (1995) Programmed cell death and Bcl-2 protection in very low oxygen. *Nature* 374:814–816
- Jacobson MD, Burne JF, Raff MC (1994) Mechanisms of programmed cell death and Bcl-2 protection. *Biochem Soc Trans* 22:600–602
- Jallot E, Nedelec JM, Grimault AS, Chassot E, Laquerriere AG, Laquerriere P, Maquin DL (2005) STEM and EDXS characterisation of physico-chemical reactions at the periphery of sol-gel derived Zn-substituted hydroxyapatites during interaction with biological fluids. *Colloids Surf Biointerfaces* 42:205–210
- Jana AK, Agarwal S, Chatterjee SN (1990) The induction of lipid peroxidation in liposomal membrane by ultrasound and the role of hydroxyl radicals. *Radiat Res* 124:7–14
- Jiang W, Kim BY, Rutka JT, Chan WC (2008) Nanoparticle-mediated cellular response is size-dependent. *Nat Nanotechnol* 3:145–150
- Jntema KI, Heuvelsland WJM, Dirix CAMC, Sam AP (1994) Hydroxyapatite protein drugs for biocontrolled release of protein drugs. *Int J Pharma* 112:215–224
- Kanagalakshmi K, Premanathan M, Priyanka R, Hemalatha B, Vanangamudi A (2010) Synthesis, anticancer and



- antioxidant activities of isoflavanone and 2,3-diarylchromanones. *Eur J Med Chem* 45:2447–2452
- Kasemets K, Ivask A, Dubourguier HC, Kahru A (2009) Toxicity of nanoparticles of ZnO, CuO and TiO<sub>2</sub> to yeast *Saccharomyces cerevisiae*. *Toxicol In Vitro* 23:1116–1122
- King RW, Jackson PK, Kirschner MW (1994) Mitosis in transition. *Cell* 79:563–571
- Kruman I, Bruce-Keller AJ, Bredesen D, Waeg G, Mattson MP (1997) Evidence that 4-hydroxynonenal mediates oxidative stress-induced neuronal apoptosis. *J Neurosci* 17:5089–5100
- Lazebnik YA, Kaufmann SH, Desnoyers S, Poirier GG, Earnshaw WC (1994) Cleavage of poly (ADP-ribose) polymerase by a proteinase with properties like ICE. *Nature* 371:346–347
- Lee BS, Park K, Park S, Kim GC, Kim HJ, Lee S et al (2010) Tumor targeting efficiency of bare nanoparticles does not mean the efficacy of loaded anticancer drugs: importance of radionuclide imaging for optimization of highly selective tumor targeting polymeric nanoparticles with or without drug. *J Control Release* 147:253–260
- Li B, Guo B, Fan H, Zhang X (2008) Preparation of nano-hydroxyapatite particles with different morphology and their response to highly malignant melanoma cells *In vitro*. *Appl Surf Sci* 255:357–360
- Lifeng Qi, Zirong Xu, Minli Chen (2001) *In vitro* and *in vivo* suppression of hepatocellular carcinoma growth by chitosan nanoparticles. *Eur J Cancer* 43:184–193
- Liu ZS, Tang SL, Ai ZL (2003) Effects of hydroxyapatite nanoparticles on proliferation and apoptosis of human hepatoma BEL-7402 cells. *World J Gastroenterol* 9:1968–1971
- Long TC, Saleh N, Tilton RD, Lowry GV, Veronesi B (2006) Titanium dioxide (P25) produces reactive oxygen species in immortalized brain microglia (BV2): implications for nanoparticle neurotoxicity. *Environ Sci Technol* 40:4346–4352
- Loo DT, Copani A, Pike CJ, Whittemore ER, Walencewicz AJ, Cotman CW (1993) Apoptosis is induced by beta-amyloid in cultured central nervous system neurons. *Proc Natl Acad Sci USA* 90:7951–7955
- Loo SCJ, Siew YE, Ho S, Boey FYC (2008) Synthesis and hydrothermal treatment of nanostructured hydroxyapatite of controllable sizes. *J Mater Sci Mater Med* 19:1389–1397
- Lovric J, Cho SJ, Winnik FM, Maysinger D (2005) Unmodified cadmium telluride quantum dots induce reactive oxygen species formation leading to multiple organelle damage and cell death. *Chem Biol* 12:1227–1234
- Manivannan A, Glaspell G, Dutta P (2008) Synthesis of nanocrystalline TiO<sub>2</sub> particles and their structural characteristics. *J Clust Sci* 19:391–399
- Marchetti P, Castedo M, Susin SA, Zamzami N, Hirsch T, Macho A et al (1996) Mitochondrial permeability transition is a central coordinating event of apoptosis. *J Exp Med* 184:1155–1160
- Mateus AYP, Ferraz MP, Monteiro FJ (2007) Microspheres based on hydroxyapatite nanoparticles aggregates for bone regeneration. *Key Eng Mater* 330–332:243–246
- Millar JB, Blevitt J, Gerace L, Sadhu K, Featherstone C, Russell P (1997) P55cdc25 is a nuclear protein required for the initiation of mitosis in human cells. *Proc Nat Acad Sci USA* 88:10500–10504
- Molinari M (2000) Cell cycle checkpoints and their inactivation in human cancer. *Cell Prolif* 33:261–274
- Mosmann T (1983) Rapid colorimetric assay for cellular growth and survival: application to proliferation and cytotoxicity assays. *J Immunol Methods* 65:55–63
- Nicholson DW, Ali A, Thornberry NA, Vaillancourt JP, Ding CK, Gallant M et al (1995) Identification and inhibition of the ICE/CED-3 protease necessary for mammalian apoptosis. *Nature* 376:37–43
- Oltvai ZN, Millman CL, Korsmeyer SJ (1993) Bcl-2 heterodimerizes *in vivo* with a conserved homolog, Bax, that accelerates programmed cell death. *Cell* 74:609–619
- Ong HT, Loo JSC, Boey FYC, Russell SJ, Ma J, Peng KW (2008) Exploiting the high affinity phosphate-hydroxyapatite nanoparticles interaction for delivery of radiation and drugs. *J Nanopart Res* 10:141–150
- Premanathan M, Karthikeyan K, Jeyasubramanian K, Manivannan G (2011) Selective toxicity of ZnO nanoparticles toward Grampositive bacteria and cancer cells by apoptosis through lipid peroxidation. *Nanomedicine. NBM* 7:184–192
- Qi LF, Xu ZR, Li Y, Jiang X, Han XY (2005) *In vitro* effects of chitosan nanoparticles on proliferation of human gastric carcinoma cell line MGC803 cells. *World J Gastroenterol* 11:5136–5141
- Rao L, White E (1997) Bcl-2 and the ICE family of apoptotic regulators: making a connection. *Curr Opin Genet Dev* 7:52–58
- Reeves JF, Davies SJ, Dodd NJF, Jha AN (2007) Hydroxyl radicals (OH<sup>•</sup>) are associated with titanium dioxide (TiO<sub>2</sub>) nanoparticle-induced cytotoxicity and oxidative DNA damage in fish cells. *Mutat Res* 640:113–122
- Reibeiro CC, Barrias CC, Barbosa MA (2004) Calcium phosphate-alginate microspheres as enzyme delivery matrix. *Biomaterials* 25:4363–4373
- Robert D, Weber JV (1999) Titanium dioxide synthesis by sol gel methods and evaluation of their photocatalytic activity. *J Mater Sci Lett* 18:97–98
- Schulze-Osthoff K, Walczak H, Droge W, Krammer PH (1994) Cell nucleus and DNA fragmentation are not required for apoptosis. *J Cell Biol* 127:15–20
- Sheng HU, Yuhua YAN, Youfa W, Xianying CAO, Shipu LI (2005) Dioxide nanoparticle absorbed by hepatoma cells *in vitro*. *J Wuhan Uni Tech Mater Sci Ed* 20:31–34
- Siegel RW, Ramasamy S, Hahn H, Zongquan LI, Ting LU, Gronsky R (1988) Synthesis, characterization, and properties of nanophase TiO<sub>2</sub>. *J Mater Res* 3:1367–1372
- Smits VA, Klompaker R, Vallenius T, Rijksen G, Mäkela TP, Medema RH (2000) P21 inhibits Thr161 phosphorylation of cdc2 to enforce the G2 DNA damage checkpoint. *J Biol Chem* 275:30638–30643
- Subramani K, Hosseinkhani H, Khraisat A, Hosseinkhani M, Pathak Y (2009) Targeting nanoparticles as drug delivery systems for cancer treatment. *Curr Nanosci* 5:134–140
- Tewari M, Quan LT, O'Rourke K, Desnoyers S, Zeng Z, Beidler DR et al (1995) Yama/ CPP32 beta, a mammalian homolog of CED-3, is a CrmA-inhibitable protease that cleaves the death substrate poly (ADP-ribose) polymerase. *Cell* 81:801–809

- Thornberry NA, Lazebnik Y (1998) Caspases: enemies within. *Science* 281:1312–1316
- Tran TH, Nosaka AY, Nosaka Y (2006) Adsorption and photocatalytic decomposition of amino acids in TiO<sub>2</sub> photocatalytic systems. *J Phys Chem B* 110:25525–25531
- Wang C, Cao S, Tie X, Qiu B, Wu A, Zheng Z (2011) Induction of cytotoxicity by photoexcitation of TiO<sub>2</sub> can prolong survival in glioma-bearing mice. *Mol Biol Rep* 38:523–530
- Wente SR (2000) Gatekeepers of the nucleus. *Science* 288:1374–1377
- Wilson JW, Booth C, Potten CS (1998) Apoptosis gene. Kluwer, Boston
- Xia T, Kovochich M, Brant J, Hotze M, Sempf J, Oberley T et al (2006) Comparison of the abilities of ambient and manufactured nanoparticles to induce cellular toxicity according to an oxidative stress paradigm. *Nano Lett* 6:1794–1807
- Yang J, Liu X, Bhalla K, Kim CN, Ibrado AM, Cai J et al (1997) Prevention of apoptosis by Bcl-2: release of cytochrome c from mitochondria blocked. *Science* 275:1129–1132
- Yin MZ, Han YC, Bauer IW, Chen P, Shi-Pu et al (2006) Effect of hydroxyapatite nanoparticles on the ultrastructure and function of hepatocellular carcinoma cells In vitro. *Biomed Mater* 1:38–41
- Yin MZ, Cao XY, Li SP (2010) The pathway of HAP nanoparticle uptake into hepatoma carcinoma cells. *Front Mater Sci China* 4:376–381
- Zar JH (1996) Biostatistical analysis. Prentice Hall, USA, p 662